River flow 2008- Altinakar, Kokpinar, Gogus, Tayfur, Kumcu & Yildirim (eds)
 ISBN 978-605-60136-2-1

Experimental study of plunging turbidity currents in reservoirs

E. Alves
Hydraulics and Environment Department, Laboratório Nacional de Engenharia Civil (LNEC), Lisbon, Portugal

J. González
Department of Civil Engineering, University of Chile, Santiago, Chile

P. Freire
Hydraulics and Environment Department, Laboratório Nacional de Engenharia Civil (LNEC), Lisbon, Portugal

A. H. Cardoso
Department of Civil Engineering and Architecture, Instituto Superior Técnico, Lisbon, Portugal

ABSTRACT
Laboratory experiments were conducted to investigate the hydraulic behaviour of plunging turbidity currents in reservoirs. One-dimensional turbidity currents driven by uniform non-cohesive sediment (silica flour) were generated in a 16.5m long, 0.3m wide and 0.75m high channel. Measurements of velocity profiles, suspended sediment concentration profiles and grain size distributions provided important insights into the spatial evolution of turbidity currents structure. The dimensional velocity profiles collapsed in a single curve confirming the similarity to a wall jet velocity profile. Downstream the plunge region, the spanwise evolution of the mean velocity profiles reveals that the point of maximum velocity increases gradually, approaching a constant value of 30% of the current thickness, which corresponds to a fully developed wall region. The study also shows the existence of a dimensional sediment concentration profile for each particle size.

Keywords: Turbidity currents, plunging region, laboratory experiments, wall region, jet region

1 INTRODUCTION

Turbidity currents occur when a sediment-laden flow enters a reservoir and plunges beneath the clear water, forming a dense underflow that travels downstream along the bottom of the reservoir. As long as the difference in density between the inflow and the reservoir ambient water remains sufficiently high, the turbidity current may sustain itself and reach the dam, where the suspended sediments will settle.

Laboratory studies of turbidity currents have focused on the mean flow properties and on the vertical structure of the currents, namely, the shape of the velocity and suspended sediment concentration profiles (Parker *et al.* 1987, Altinakar 1988, García 1993), among other characteristics. However, in these particularly laboratory studies, turbidity currents were simulated using a sluice gate and, therefore, the plunging phenomena were not considered.

In nature, the plunging phenomenon plays an important role in the occurrence and development of turbidity currents. The specific analysis of plunging conditions has been investigated theoretically and experimentally by several authors including, Akiyama and Stefan (1984) and Lee and Yu (1997).

This paper examines the hydrodynamics of plunging turbidity currents based on laboratory experiments (Alves, 2008). The plunging is created by the abrupt change in the bottom slope. Selected topics include the vertical velocity and suspended sediment concentration profiles within the current. Furthermore, sediment gradation and the effect of mixing in the plunge region on the current development are also analysed.

2 EXPERIMENTAL FACILITIES

2.1 *Description*

The experiments were carried out in a facility especially built to perform turbidity currents studies, located at the Hydraulics and Environment Department of LNEC. The channel (Fig. 1) is 0.30 m wide, 16.45 m long and 0.75 m deep (maximum).

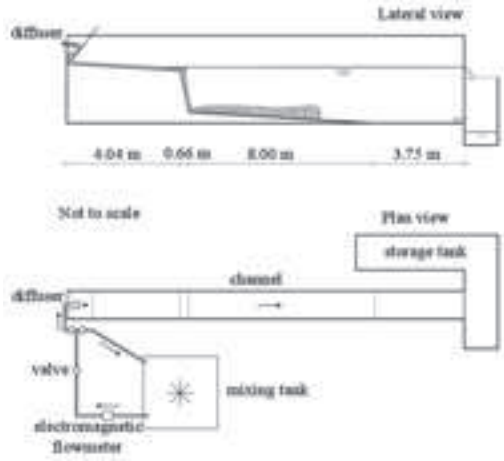

Figure 1. Schematic view of the experimental facility.

The channel bottom profile was designed with a special configuration to make it possible to simulate plunging turbidity currents in reservoirs. An upstream 4.04 m long reach with a bottom slope of 0.8º simulates the river approaching a reservoir. An abrupt change in the bottom profile was produced by a ramp with a slope of 30º representing the steepness of the front delta deposits in the upper part of the reservoir. Downstream, an 8 m long reach with a slope of 0.8º and a final horizontal 3.75 m long bed formed the reservoir in which currents developed.

Adjacent to the flume, a mixing tank with a maximum capacity of 2.95 m^3 was used to prepare and store the mixture of water and sediment. Inside the tank, a propeller-type mixer maintained the sediment in suspension. Before the beginning of the experiments, the water-sediment mixture was pumped from the tank, passed through a calibrated electromagnetic flow meter and returned to the tank. After regulation of the pump, the simultaneous operation of two valves allowed to cut the flow in the return circuit and to open the supply circuit entrance to the channel. The water-sediment mixture was then introduced as a stream flow into the channel, which had been previously filled with clear tap water, thus forming a reservoir. At the downstream section of the flume, an overflow weir and a drain valve were used to maintain a constant water level in the flume.

2.2 *Measurements and equipment*

Twenty runs were performed in this study. For each run, a number of variables were measured to ensure constant inlet conditions and to characterise turbidity currents development, namely: discharge of the water-sediment mixture, velocity and suspended sediment concentration profiles, grain size distribution, current front velocity, water level inside the flume and water temperature in the mixing tank and in the flume.

The discharge of water-sediment mixture was measured with an electromagnetic flow meter to an accuracy of 3%.

To ensure that turbidity currents were produced by an excess of density due to the presence of suspended sediments rather than to a difference in temperature, before the beginning of the experiments, the temperature of the mixture and of the ambient water in the flume was measured with a thermometer.

Velocity profiles were measured along the main axis of the flume, at seven stations, using an Ultrasound Velocity Profiling system (UVP). The location of the transducers (designated T1 to T7) was defined to cover the region of plunging (T1 in x = 4.3m), the region of slope transition (T2 in x = 4.7 m) and the development of the turbidity underflow (T3 to T7 in $5.2\text{m} \le x \le 11.7\text{m}$). Distances refer to the entrance of the water-sediment mixture in the channel (diffuser in Fig.1).

The measurement axis of the velocity profiles defined an angle of 20º with the vertical. Transducers of 4 MHz were used covering a maximum measurable depth of 549.82 mm and a maximum velocity of 249 mm/s. For each profile, 360 measuring volumes with a 1.48 mm of length were defined.

Typically, during a 10 min experiment, 4158 velocity profiles were measured (594 at each location). In each cycle of measurements, 3 consecutive profiles were taken on a transducer before switching to the next one. These cycles were continuously repeated throughout the entire experiment. The sampling time for each profile was set equal to 68 ms and the delay time between the transducers to 10 ms.

Suspended sediment concentration profiles were obtained at two measuring stations by the filtration of siphoned samples collected at different heights above the bed. Two rakes of eight point samplers each were built. The sampler's tips were made of thin rigid plastic tubes and were connected by flexible plastic tubes to 500 ml bottles. For each sample, suspended sediment concentration was determined by gravimetric methods using 0.45µm Milipore

filters. Sediment grain size analysis was performed by laser diffraction.

To control the inlet conditions, suspended sediment concentrations and the particle size distribution were obtained from point samples collected at the flume entrance. In some experiments, point samples were also collected at the plunging region.

2.3 *Experimental conditions*

The sediment used to generate turbidity currents was a silica powder with a specific gravity of 2.65 and a median diameter ranging from 12.7 μm to 30 μm.

Table 1 summarizes the range of inlet conditions covered during the laboratory experiments. In this table, Q_0 = inflow water-sediment discharge, C_{s0} = inflow suspended sediment concentration, ΔT = absolute value of the temperature difference between the ambient fluid and the water-sediment mixture, D_{50} = median diameter of the inflow sediment, H = maximum height of the ambient fluid inside the channel, and B_0= initial buoyancy flux, which is defined as

$$B_0 = gRC_s q_0 \tag{1}$$

with g = acceleration due to gravity, R = submerged specific gravity (1.65) and q_0 = inflow discharge per unit width.

Table 1. Range of inlet conditions considered in the experiments

Parameter	Range
Q_0(l/s)	0.70 – 2.04
C_{S0}(%)	0.11 – 1.25
C_{S0} (g/l)	2.80 – 33.13
B_0 (cm^3/s^3)	40.6 – 1158.9
D_{50} (μm)	12.7 – 30.0
ΔT(ºC)	0.0 – 1.3
H (m)	0.54

Values of the temperature difference between the ambient fluid and the water-sediment mixture were less than 1.3ºC, which corresponds to density differences of 0.3 g/l.

The Richardson number, defined as

$$R = gRC_{s0}h_0 / U_0^2 \tag{2}$$

where h_0= inflow height and U_0 = inflow velocity, was less than the unity, corresponding to supercritical flow conditions on the upper part of the reservoir.

3 DESCRIPTION OF THE FLOW

When the mixture of water and sediment reaches the delta zone, it plunges into the bottom of the channel and flows as a dense underflow or turbidity current (Fig. 2). The position of the plunge line is determined by the inflow water-sediment discharge, the suspended sediment concentration and the water level and geometry of the reservoir.

Figure 2. Plunging turbidity current experiment.

In the experiments reported in this paper, the plunging occurs immediately after the slope break due to the sudden change in the flow depth. Although, initially, the inflow tended to push forward the stagnant ambient water, the plunge line was established just a few seconds after the inflow mixture had met the ambient water (Fig.2).

In some experiments, the plunge region was characterised by a high level of turbulence, and the formation of vortexes could lead, in some instances, to some distortion of the position of the plunge line (Fig.3). This aspect, which was more significant in the case of experiments with high values of B_0, is attributed to the recirculation flow on the upper part of the reservoir and to the process of mixture of the underflow with the ambient water.

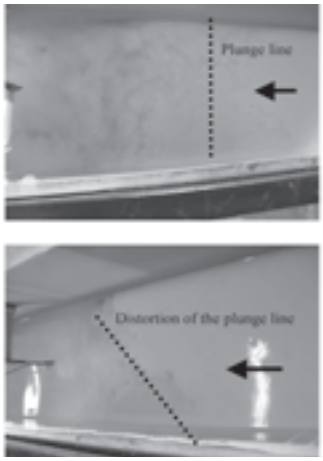

Figure 3. Aspects of the plunge line observed in some experiments with high values of B_0 (pictures taken from above the channel).

In other experiments, part of the inflow sediments remained in suspension near the surface of the ambient water in the plunge region, and it was not always easy to identify the position of the plunge line through visual observations.

After plunging, the underflow goes from the steep slope of the ramp (30º) into a long reach with a slope of 0.8º (0.014). In this slope transition, an increase of the current thickness was observed but no change in the flow regime could be confirmed. For the currents where suspended sediment concentration profiles were measured, the Richardson number (R) remained less than the unity, which corresponds to a supercritical turbid flow regime.

Once the turbidity current has started, the formation of a distinct head that travelled along the channel was observed. As the front propagated, a complex pattern of lobes and clefts was formed at the foremost part of the head. In plan, the front is considered as two-dimensional in its large-scale features.

4 DISCUSSION

4.1 *Velocity profiles*

Fig. 4 shows the typical evolution of the time-averaged velocity profiles. The velocity profile obtained with the transducer T1 is located at the plunge region, where the turbid underflow is initiated. Downstream, a high velocity underflow is observed at the base of the ramp (T2). Further downstream, after the slope transition, a decrease in the maximum velocity is observed (T3) and the velocity profile depicts a large reverse flow produced by the shear stress at the interface of the two fluids with different densities. Beyond this section, the discharge of the return flow seems to decay rapidly, reaching a stable value that is maintained along the channel (T4 to T7).

In previous investigations (Altinakar 1988), it was observed that the velocity profiles of turbidity currents are similar to the ones of a wall jet. According to Rajaratnam (1976), the velocity distribution of a wall jet consists of two distinct flow regions. The region between the wall and the point of maximum velocity is a boundary layer and the region above it is the free mixing region.

This seems to be also the case in the present study, in which, within the body of turbidity current the velocity increases from zero at the wall to a maximum value at h_m and then decreases to zero at a distance h_t.

For turbidity currents, the wall region and the jet region are defined, respectively, from the bottom up to the point of maximum velocity and from this point to the position of the interface between the current and the ambient water (Altinakar *et al.* 1996).

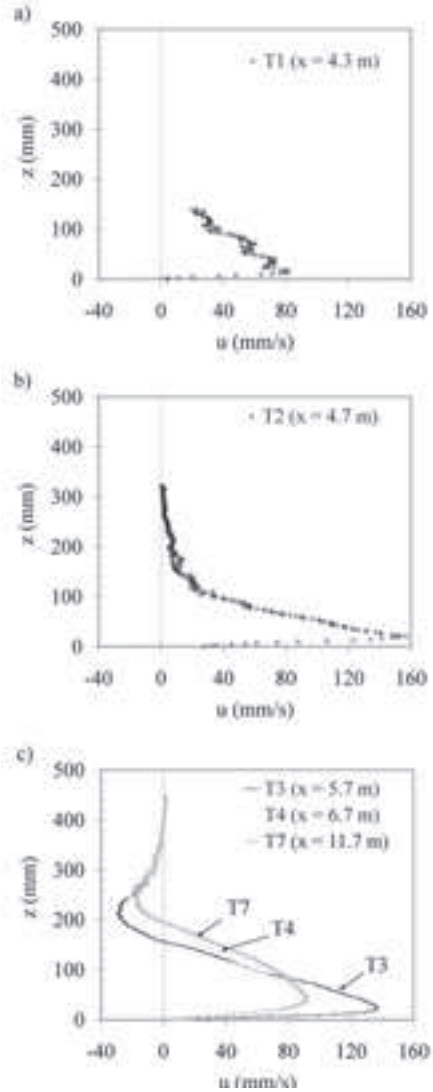

Figure 4. Typical velocity profiles observed in turbidity currents: a) plunge region, b) initiation of the underflow, and c) development of the turbidity currents.

To obtain dimensionless velocity profiles, Altinakar (1988) proposed the use of the dimensionless heights, z/h_m, in the wall region, and $(z-h_m)/(h-h_m)$, in the jet region, where z is the vertical coordinate, h_m is the height of the point of maximum velocity

(U_{max}) and h is the current height. The dimensionless velocity is taken as u/U_{max} .

The turbidity current height (h), the depth-averaged velocity (U) and the depth-average suspended sediment concentration (C_S) were determined using Ellison and Turner (1959) integral scales:

$$Uh = \int_0^{hr} u\,dz \tag{3}$$

$$U^2 h = \int_0^{hr} u^2\,dz \tag{4}$$

$$C_s U h = \int_0^{hr} u c_s\,dz \tag{5}$$

Using the velocity and height scales proposed by Altinakar (1988), all velocity profiles downstream the plunging region collapsed into a single curve, as Fig. 5 shows. This is in agreement with previous works of Altinakar (1988) and Altinakar *et al.* (1996).

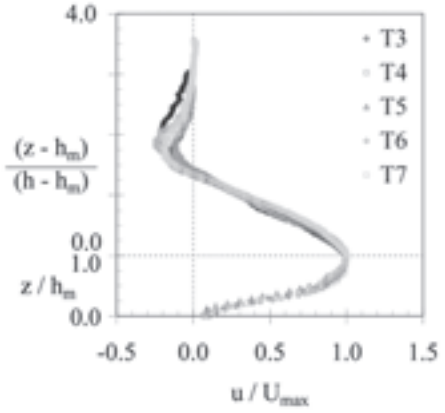

Figure 5. Dimensionless velocity profiles downstream the plunge region.

4.2 *Evolution in currents height*

Fig. 6 shows the variations in h_m, h and h_t with x. The same figure also presents the height $h_t + h_r$, where h_r is the height of the return flow. It can be observed that the height of turbidity currents increases to a value that remains almost constant along the flume. The same conclusion can be drawn for h_t and $h_t + h_r$.

4.3 *Spanwise evolution of the wall layer*

An important characteristic of the velocity profiles measured in the present study is the evolution of the height h_m of the point of maximum velocity along the channel. It is found that h_m increases gradually and approaches a constant value near the end of the measuring reach (Fig. 6). Such flow configuration is associated with the generation of turbulence at the bed as currents evolve with distance.

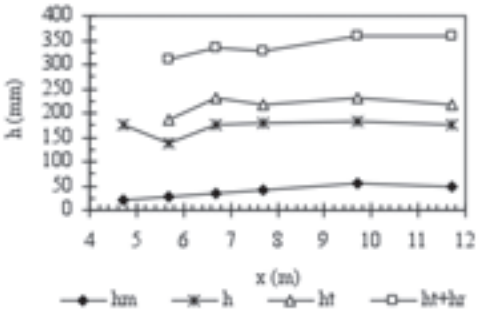

Figure 6. Evolution of h_m, h, h_t and $h_t + h_r$ along the channel.

Based on the present laboratory data, the relation between the height of the point of maximum velocity and the current height, h_m / h, was found to vary between 0.17±0.04 (x = 4.7 m) and the constant value of 0.31±0.03 ($x \geq$ 9,7 m). The latter corresponds to what seems to be a fully developed wall region.

Although Altinakar (1988) and García (1993) referred to the evolution of h_m / h with x in their studies, they were unable to fully illustrate it, due to the limitations in the velocity measuring equipment used. Altinakar *et al.* (1996) presented an average value of h_m / h equal to 0.3, based on velocity profiles measured on three sections. García (1993) observed that the average value of h_m / h is different for supercritical and subcritical flows.

4.4 *Suspended sediment concentration profiles*

In this study, suspended sediment concentration profiles were measured on two stations located downstream the slope transition. Fig. 7 shows a typical distribution of suspended sediment concentration observed in the present study. The shape of the profiles reveals a significant increase in concentration with a maximum value near the bottom. These profiles are similar to those obtained by Altinakar (1988) and García (1990).

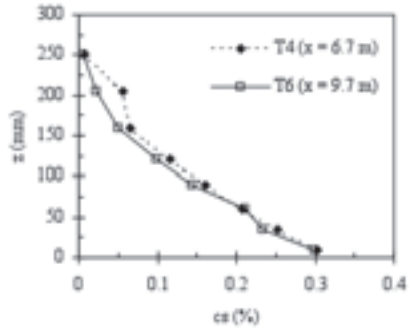

Figure 7. Suspended sediment concentration profiles at two measuring stations.

The ratio of bed concentration, c_b, to the average current concentration, C_S, was found to vary between 1.50 and 1.95, which is consistent with other experimental data (Parker *et al.* 1987, Altinakar 1988 and García 1990).

The collapse of the non-dimensional concentration profiles, obtained using the dimensional scales proposed by Altinakar (1996), is very good as shown in Fig. 8. However, the few data measured below the point of maximum velocity inhibits the correct description of the non-dimensional profile within the wall region.

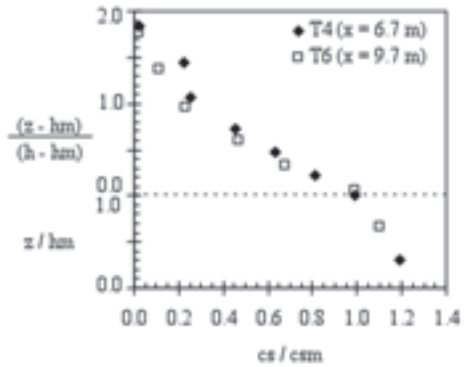

Figure 8. Self-similarity of suspended sediment concentration profiles.

A strong decay of suspended sediment concentration was observed upstream of section x = 6.7 m (T4). Most of this decay has presumably occurred in the plunge region, as a result of the mixing process between the current and the ambient fluid. In fact, the average values of suspended sediments concentrations in section x = 6.7 m, were found to be a mere fraction (22% to 41%) of the initial inflow sediment concentration. Downstream, between sections x = 6.7 m (T4) and x = 9.7 m (T6), a smaller reduction in the sediment concentration was observed (5% to 30%), due to the deposition of the coarser particles and due to water entrainment into the current.

4.5 *Vertical sediment size distribution*

Sediment size distribution was determined for each sample where sediment concentration was measured. When turbidity currents flows downstream, a gradation of the suspended sediment size is expected to occur. Furthermore, a vertical grain sorting is also expected to take place within the current body.

For descriptive purposes, the range of grain sizes of the inflow suspended sediments was divided into classes, and a representative diameter (D_i) was defined for each class (Table 2). Then, the sediment concentrations (c_{si}) associated to each representative diameter (D_i) were determined at different heights. The results are shown in Fig. 9, for one of the measuring sections of the flume.

The non-uniformity of the sediment size distribution within the body of the current is confirmed. The small particles tend to be more uniformly distributed within the current, whereas the coarser particles tend to be present mainly near the bottom.

Table 2. Classes of sediment sizes ranges and representative diameters.

Class (μm)	Representative diameter, D_i (μm)
1.1 – 3.6	2
3.6 – 6.6	5
6.6 – 10.5	8
10.5 – 16.6	13
16.6 – 26.2	21
26.2 – 41.4	33
41.4 – 65.5	52
65.5 – 103.6	82
103.6 – 190.8	141

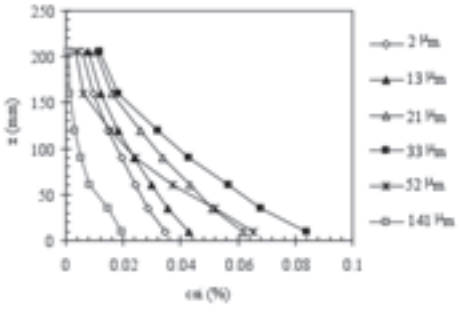

Figure 9. Vertical distribution of suspended sediment concentrations associated with different diameters.

Fig. 10 presents the non-dimensional concentration profiles associated with the representative diameters 21 μm and 52 μm. In these figures, c_{sim}, is the concentration of the sediment of size D_i at the point of maximum velocity. The non-dimensional concentration profiles are found to be similar for each particle size. In the jet region of the turbidity current (above the point of maximum velocity), the concentration seems to decrease more rapidly with z than in the wall region.

Longitudinal sediment size gradation was also observed, as a result of the sediment deposition along the channel (Fig. 11). A significant decrease in the concentration associated to each representative diameter was observed between the inflow and T4 sections. Between sections T4 and T6, the reduction in the concentration affects mainly particles with D_i greater than 21 μm.

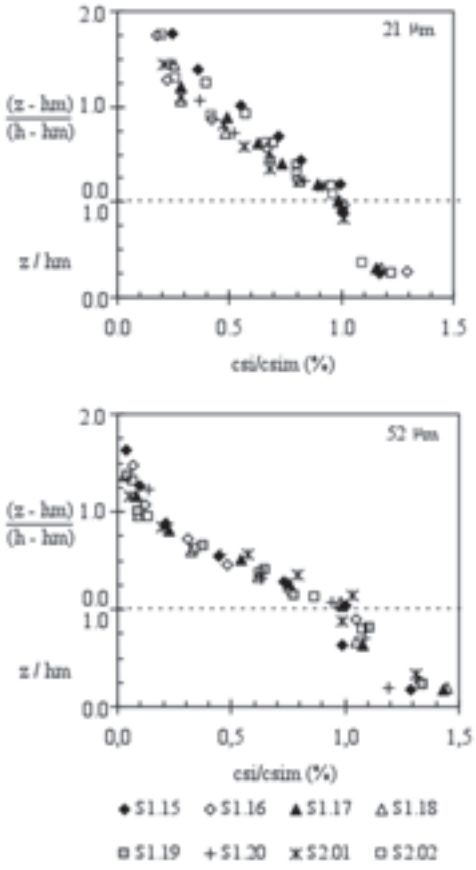

Figure 10. Dimensional suspended sediment concentration profiles associated with particles of 21 μm and 52 μm for different runs (S1.15 to S2.02).

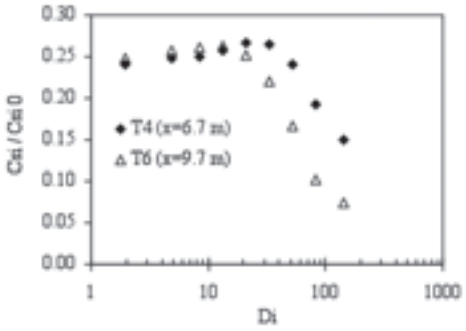

Figure 11. Sediment size gradation along the channel.

4.6 *Mixing in the plunge region*

The process of mixing between the underflow and the ambient flow is mainly due to two mechanisms (Akiyama and Stefan, 1984). The first consists of the water entrainment into the current due to the instability in the interface. This process continuously occurs as the current flows downstream. The second is the mixing generated in the plunge region due to a sudden change in the bed slope and in the flow depth. As referred to by the authors, the latter process is particularly important in steep slopes.

Akiyama and Stefan (1984) defined the mixing coefficient of ambient fluid into the underflow in the plunge region as

$$\gamma = \frac{Uh}{q_0} - 1 \qquad (6)$$

where q_0 is the inflow discharge per unit width.

For the present study, values of γ in the range of 0.38 to 1.79 were found. These values are consistent with those estimated by Kostic and Parker (2003b), who obtained values of γ between 0.5 and 1.5, in a experimental facility similar to the one used in this study. It should be mentioned that these values are much higher than those usually reported in the literature for mild slopes (0.1-0.2, according to Lee and Yu, 1997). The differences can be attributed to the effect of the steepness of the channel bottom on the mixing process in the plunge region (Akiyama and Stefan, 1984).

5 CONCLUSIONS

An experimental study was conducted to investigate the hydrodynamics of plunging turbidity currents in reservoirs. The following main conclusions can be drawn.

The dimensionless velocity profiles within the body of the turbidity current collapsed in a single curve, when the dimensionless heights, z/h_m , for the wall layer, and $(z-h_m)/(h-h_m)$, in the jet region, were adopted. These results confirm Altinakar's *et al.* (1996) proposal for the description of the dimensionless velocity profiles.

Velocity profiles provided new information about the spatial evolution of the turbidity current wall layer. It was found that the point of maximum velocity increases gradually, approaching a constant value of 30% of the current thickness, which corresponds to a fully developed wall layer.

The collapse of the dimensionless concentration profiles associated with a given diameter was obtained. It is shown that the decrease with z in the sediment concentration on the upper layer of the turbidity current depends on the particle size of the sediment. A strong reduction in the concentration of particles with a diameter greater than 21 μm was observed along the channel.

The intense mixing created in the plunge region due to the sudden change in flow depth plays an important role in the water entrainment into the current and in its downstream evolution. A drastic reduction in the inflow of suspended sediment concentration in this region was observed. Downstream the slope transition, the current thickness increases gradually approaching an almost constant value; between sections T4 and T6, a small reduction in sediment concentration occurs.

ACKNOWLEDGEMENTS

The authors acknowledge the financial support of the Portuguese Foundation for Science and Technology under the research project POCTI/ECM/45778/2002 – "Sedimentation in reservoirs by turbidity currents". Authors are also grateful to Mr. Mateus Mendonça for his assistance during the experiments and to the technical staff of LNEC for their support with the construction of the experimental facility.

REFERENCES

Altinakar, M. 1988. *Weakly depositing turbidity currents*. These Nº 738, Ecole Polytechnique Federale de Lausanne.

Atinakar, M., Graf, W., and Hopfinger, E. 1996. Flow structure in turbidity currents. *Journal of Hydraulic Research*, Vol. 34, No. 5, 713-718.

Alves, E. 2008. *Sedimentation in reservoirs by turbidity currents.* PhD Thesis (in Portuguese), Instituto Superior Técnico, Lisboa. (in preparation)

Akiyama, J., and Stefan, H. 1984. Plunging flow into a reservoir: theory. *Journal of Hydraulic Engineering*, Vol. 110, No. 4, 484-499.

Ellison, T. H. and Turner, J. S. 1959. Turbulent entrainment in stratified flows. *Journal of Fluid Mechanics*, Vol. 6, 423-448.

García, M. 1990. *Depositing and eroding sediment-driven flows: turbidity currents*. University of Minnesota, St. Anthony Falls Hydraulic Laboratory, Project Report No. 306.

García, M. 1993. Hydraulic jumps in sediment-driven bottom currents. *Journal of Hydraulic Engineering*, Vol. 119, No. 10, 1094-1117.

Kostic, S., and Paker, G. 2003. Progradational sand-mud deltas in lakes and reservoirs. Part 2. Experiment and numerical simulation. *Journal of Hydraulic Research*, Vol. 41, No. 2, 141-152.

Lee, H.-Y., and Yu, W.-S. 1997. Experimental study of reservoir turbidity current. *Journal of Hydraulic Engineering*, Vol. 123, No. 6, 520-528.

Parker, G., García, M., Fukushima, Y., and Yu, W. 1987. Experiments on turbidity current over an erodible bed. *Journal of Hydraulic Research*, Vol. 25, pp. 123-147.

Parker, G., and Toniolo, H. 2007. Note on the analysis of plunging of density flows. *Journal of Hydraulic Engineering*, Vol. 133, No. 6, Technical note, 690- 694.

Rajaratnam, N. 1976. *Turbulent jets*. Amsterdam: Elsevier.